Available online at www.sciencedirect.com

ScienceDirect

Energy Procedia 94 (2016) 531 – 543

Energy Procedia

13th Deep Sea Offshore Wind R&D Conference, EERA DeepWind'2016, 20-22 January 2016, Trondheim, Norway

# Aerodynamic modeling of floating vertical axis wind turbines using the actuator cylinder flow method

Zhengshun Cheng[a,b,c,*], Helge Aagaard Madsen[d], Zhen Gao[a,b,c], Torgeir Moan[a,b,c]

[a]*Department of Marine Technology, Norwegian University of Science and Technology (NTNU), Trondheim, NO-7491, Norway*
[b]*Centre for Ships and Ocean Structures (CeSOS), NTNU, Trondheim, NO-7491, Norway*
[c]*Centre for Autonomous Marine Operations and Systems (AMOS), NTNU, Trondheim, NO-7491, Norway*
[d]*Department of Wind Energy, Technical University of Denmark, Roskilde, 4000, Denmark*

**Abstract**

Recently the interest in developing vertical axis wind turbines (VAWTs) for offshore application has been increasing. Among the aerodynamic models of VAWTs, double multi-streamtube (DMST) and actuator cylinder (AC) models are two favorable methods for fully coupled modeling and dynamic analysis of floating VAWTs in view of accuracy and computational cost. This paper deals with the development of an aerodynamic code to model floating VAWTs using the AC method developed by Madsen. It includes the tangential load term when calculating induced velocities, addresses two different approaches to calculate the normal and tangential loads acting on the rotor, and proposes a new modified linear solution to correct the linear solution. The effect of dynamic stall is also considered using the Beddoes-Leishman dynamic stall model. The developed code is verified to be accurate by a series of comparisons against other numerical models and experimental results. It is found that the effect of including the tangential load term when calculating induced velocities on the aerodynamic loads is very small. The proposed new modified linear solution can improve the power performance compared with the experiment data. Finally, a comparison of the developed AC method and the DMST method is performed using two rotors and shows that the AC method can predict more accurate aerodynamic loads and power than the DMST method, at least for the considered rotors.


Peer-review under responsibility of SINTEF Energi AS

*Keywords:* Floating vertical axis wind turbine; aerodynamic modeling; actuator cylinder flow model; double multi-streamtube model

## 1. Introduction

During the 1970s and 1980s, vertical axis wind turbines (VAWTs) attracted interests of researchers mainly in USA and Canada and considerable efforts were devoted to investigate and develop the Darrieus VAWTs [9]. Commercial Darrieus VAWTs were also developed by the FloWind Corp. Due to the issues of severe fatigue damage and low power efficiency, VAWTs became less popular than horizontal axis wind turbines (HAWTs). However, as the wind farms are

* Corresponding author. Tel.: +47-73596004 ; fax: +47-73595528.
*E-mail address:* zhengshun.cheng@ntnu.no


Peer-review under responsibility of SINTEF Energi AS
doi:10.1016/j.egypro.2016.09.232

moving towards deeper waters where large floating wind turbines will be more economical, floating VAWTs have the potential to reduce the cost compared to floating HAWTs [8] and efforts devoted to investigate floating VAWTs are increasing.

Since Sandia National Laboratories started the study of vertical axis wind turbines in the 1970s, a variety of aerodynamic models have been proposed for VAWTs. These include streamtube models, actuator cylinder (AC) flow model, panel method, vortex method and computational fluid dynamics (CFD) method. The streamtube models are based on the conservation of mass and momentum in a quasi-steady flow. They equate the forces on the rotor blades to the change in the streamwise momentum through the turbine. They can be categorized into three models: single streamtube model (SST) [13], multi-streamtube model (MST) [12] and double multi-streamtube (DMST) [9] model. SST model [13] assumes that the entire rotor represented by an actuator disk is enclosed in one streamtube, MST model [12] extends the SST model by dividing the rotor into a series of adjacent streamtubes and DMST model [9] assumes that the vertical axis wind turbine can be represented by a pair of actuator disks in tandem at each level of the rotor. Up to now, the DMST model has been widely used to estimate the aerodynamic loads on VAWTs.

However, by considering a 2D VAWT rotor, Ferreira et al. [2] compares the different models for VAWTs, including the MST model, DMST model, AC [4] model, U2DiVA using panel model and CACTUS [7] using lifting line model, and reveals that the DMST model seems to be less accurate than the AC, panel and vortex models. An overview of these aerodynamic models can also be found in [11], which considers their complexity, accuracy, computational cost, suitability for optimization and aeroelastic analysis. Due to the considerations of accuracy and computational cost, the AC method seems to be the favorable method that can be used to conduct aero-hydro-servo-elastic time domain simulations of floating VAWTs.

The AC method is a quasi-steady Eulerian model developed by Madsen [4]. The model extends the actuator disc concept to an actuator surface coinciding with the swept area of the 2D VAWT. In the AC model, the normal and tangential forces $Q_n$ and $Q_t$ resulting from the blade forces are applied on the flow as volume force perpendicular and tangential to the rotor plane, respectively, as illustrated in Fig. 1. Thus the velocity induced by the normal and tangential forces $Q_n$ and $Q_t$ can be computed analytically.

The AC method has been implemented in HAWC2 [3] to conduct the fully coupled aero-hydro-servo-elastic time domain simulations of floating VAWTs. It can account for dynamic inflow, structural dynamics, tower shadow and dynamic stall. Paulsen et al. [10] performed a design optimization of the proposed DeepWind concept. An improved design has been obtained with an optimized blade profile with less weight and higher stiffness than the first baseline design.

In this paper, an aerodynamic code is developed using the AC method developed by Madsen [4] to model VAWTs for offshore application. The basic theory of the AC method will firstly be briefly presented. In the developed code, the linear solution of induced velocities will be derived by including the effect of tangential load. The effect of tangential load on the induced velocity was discussed in [5], but was ignored in the implementation of the AC method into HAWC2 [3,6]. Using the AC method, modeling of a VAWT is presented subsequently including the effect of dynamic stall via the Beddoes-Leishman dynamic stall model. Two different approaches are used to calculate the normal and tangential loads acting on the rotor . A series of simulations are conducted to verify the code by comparisons with other numerical models and experimental results . The accuracy of the present code and the effect of tangential load on the induced velocity are addressed. Finally, a comparison of the present AC method and the DMST method is performed.

## 2. Actuator cylinder flow model

Considering a 2D quasi-static flow problem as shown in Fig. 1, the basic equations are the Euler equation and continuity equation. For simplicity the equations are non-dimensionalized with the basic dimensions $R$, $V_\infty$ and $\rho$, which are rotor radius, free stream velocity and flow density, respectively. The velocity components can thus be written as

$$v_x = 1 + w_x \tag{1}$$

$$v_y = w_y \tag{2}$$

where $w_x$ and $w_y$ are local velocities representing the changes in wind speed due to the presence of the VAWT.

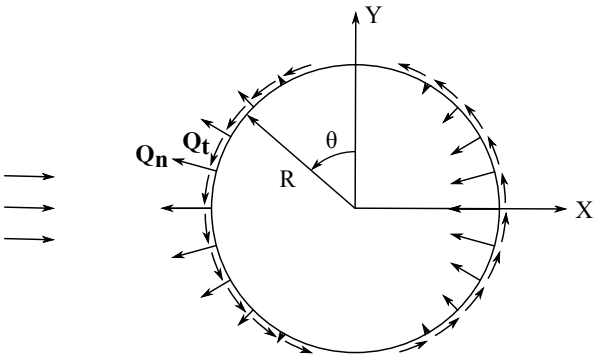


Fig. 1. The actuator cylinder flow model representation [6] of a VAWT with volume forces normal and tangential to the circle. Note that the force direction is from the VAWT onto the flow .

Based on the continuity equation and Euler equation, the velocities $w_x$ and $w_y$ are related to volume forces as well as the normal and tangential loads $Q_n$ and $Q_t$. The final velocity can be divided into a linear part which is a function of the prescribed normal and tangential loads $Q_n$ and $Q_t$ and a nonlinear part that is a function of the induced forces.

### 2.1. Linear Solution

The linear solution of the induced velocities can be analytically computed, as given by

$$w_x(f) = -p_f + \int_{-\infty}^{x} f_x dx' \tag{3}$$

$$w_y(f) = -\int_{-\infty}^{x} \frac{\partial p_f}{\partial y} dx' + \int_{-\infty}^{x} f_y dx' \tag{4}$$

where $p_f$ is the pressure given by

$$p_f = \frac{1}{2\pi} \iint \frac{f_x(x-\xi) + f_y(y-\eta)}{(x-\xi)^2 + (y-\eta)^2} d\xi d\eta \tag{5}$$

and the volume forces can be expressed as

$$f_x = -f_n \sin\theta - f_t \cos\theta \tag{6}$$

$$f_y = f_n \cos\theta - f_t \sin\theta \tag{7}$$

in which

$$Q_n(\theta) = \lim_{\epsilon \to 0} \int_{1-\epsilon}^{1+\epsilon} f_n(\theta, r) dr \tag{8}$$

$$Q_t(\theta) = \lim_{\epsilon \to 0} \int_{1-\epsilon}^{1+\epsilon} f_t(\theta, r) dr \tag{9}$$

The integration involved in Eqs. 3 and 4 should be performed item by item throughout the region where the volume forces are different from zero. For the integral part in Eq. 3, since the volume forces are non-zero only along the cylinder, the integral result depends on the position of the calculation point, as shown in Fig. 2. Detailed derivation can refer to the Appendix A.

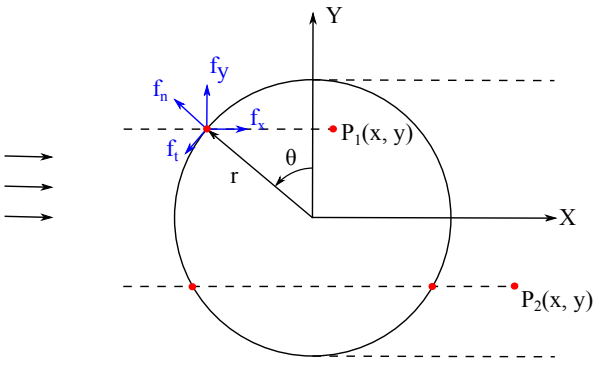


Fig. 2. The actuator cylinder flow model with volume forces

The linear solution of the induced velocities is given as follows

$$\begin{aligned} w_x(f) = &-\frac{1}{2\pi}\int_0^{2\pi} Q_n(\theta)\frac{-(x+\sin\theta)\sin\theta+(y-\cos\theta)\cos\theta}{(x+\sin\theta)^2+(y-\cos\theta)^2}d\theta \\ &-\frac{1}{2\pi}\int_0^{2\pi} Q_t(\theta)\frac{-(x+\sin\theta)\cos\theta-(y-\cos\theta)\sin\theta}{(x+\sin\theta)^2+(y-\cos\theta)^2}d\theta \\ &-(Q_n(\arccos y))^* + (Q_n(-\arccos y))^{**} \\ &-\left(Q_t(\arccos y)\frac{y}{\sqrt{1-y^2}}\right)^* - \left(Q_t(-\arccos y)\frac{y}{\sqrt{1-y^2}}\right)^{**} \end{aligned} \tag{10}$$

$$\begin{aligned} w_y(f) = &-\frac{1}{2\pi}\int_0^{2\pi} Q_n(\theta)\frac{-(x+\sin\theta)\cos\theta-(y-\cos\theta)\sin\theta}{(x+\sin\theta)^2+(y-\cos\theta)^2}d\theta \\ &-\frac{1}{2\pi}\int_0^{2\pi} Q_t(\theta)\frac{(x+\sin\theta)\sin\theta-(y-\cos\theta)\cos\theta}{(x+\sin\theta)^2+(y-\cos\theta)^2}d\theta \end{aligned} \tag{11}$$

where the term marked with $*$ in Eqs. 10 and 11 shall only be added inside the cylinder whereas in the wake behind the cylinder both the term marked with $*$ and $**$ shall be added. Compared with the results in [6], the effect of tangential load on the computed induced velocity is considered here.

Assuming that the loading is piecewise constant, the integral part in Eqs. 10 and 11 can be rewritten as

$$\begin{aligned} w_x = &-\frac{1}{2\pi}\sum_{i=1}^{i=N} Q_{n,i}\int_{\theta_i-\frac{1}{2}\Delta\theta}^{\theta_i+\frac{1}{2}\Delta\theta}\frac{-(x+\sin\theta)\sin\theta+(y-\cos\theta)\cos\theta}{(x+\sin\theta)^2+(y-\cos\theta)^2}d\theta \\ &-\frac{1}{2\pi}\sum_{i=1}^{i=N} Q_{t,i}\int_{\theta_i-\frac{1}{2}\Delta\theta}^{\theta_i+\frac{1}{2}\Delta\theta}\frac{-(x+\sin\theta)\cos\theta-(y-\cos\theta)\sin\theta}{(x+\sin\theta)^2+(y-\cos\theta)^2}d\theta \end{aligned} \tag{12}$$

$$\begin{aligned} w_y = &-\frac{1}{2\pi}\sum_{i=1}^{i=N} Q_{n,i}\int_{\theta_i-\frac{1}{2}\Delta\theta}^{\theta_i+\frac{1}{2}\Delta\theta}\frac{-(x+\sin\theta)\cos\theta-(y-\cos\theta)\sin\theta}{(x+\sin\theta)^2+(y-\cos\theta)^2}d\theta \\ &+\frac{1}{2\pi}\sum_{i=1}^{i=N} Q_{t,i}\int_{\theta_i-\frac{1}{2}\Delta\theta}^{\theta_i+\frac{1}{2}\Delta\theta}\frac{-(x+\sin\theta)\sin\theta+(y-\cos\theta)\cos\theta}{(x+\sin\theta)^2+(y-\cos\theta)^2}d\theta \end{aligned} \tag{13}$$

where $N$ is the total number of calculation points, $\Delta\theta = \frac{2\pi}{N}$ and $\theta_i = \frac{\pi}{N}(2i-1)$ for $i = 1, 2, ..., N$ .

Since only induced velocities at the cylinder are of concern, the total velocity solution at calculation point $(x_j, y_j)$ ( for $j = 1, 2, ..., N$) on the cylinder can then be rewritten as

$$w_{x,j} = -\frac{1}{2\pi}\left(\sum_{i=1}^{i=N} Q_{n,i}I_{1,i,j} + \sum_{i=1}^{i=N} Q_{t,i}I_{2,i,j}\right) - \left(Q_{n,N+1-j}\right)^* - \left(Q_{t,N+1-j}\frac{y_j}{\sqrt{1-y_j^2}}\right)^* \tag{14}$$

$$w_{y,j} = -\frac{1}{2\pi}\left(\sum_{i=1}^{i=N} Q_{n,i}I_{2,i,j} - \sum_{i=1}^{i=N} Q_{t,i}I_{1,i,j}\right) \tag{15}$$

where the terms marked with $*$ in Eqs. 14 and 15 are only added for $j > \frac{N}{2}$ (the leeward part of the AC with $x_j > 0$). $I_{1,i,j}$ and $I_{2,i,j}$ are influence coefficients in point $j$ influenced by other point $i$ and are given by

$$I_{1,i,j} = \int_{\theta_i-\frac{1}{2}\Delta\theta}^{\theta_i+\frac{1}{2}\Delta\theta} \frac{-\left(x_j+\sin\theta\right)\sin\theta + \left(y_j-\cos\theta\right)\cos\theta}{\left(x_j+\sin\theta\right)^2 + \left(y_j-\cos\theta\right)^2} d\theta \tag{16}$$

$$I_{2,i,j} = \int_{\theta_i-\frac{1}{2}\Delta\theta}^{\theta_i+\frac{1}{2}\Delta\theta} \frac{-\left(x_j+\sin\theta\right)\cos\theta - \left(y_j-\cos\theta\right)\sin\theta}{\left(x_j+\sin\theta\right)^2 + \left(y_j-\cos\theta\right)^2} d\theta \tag{17}$$

in which $x_j = -\sin(j\Delta\theta - \frac{1}{2}\Delta\theta)$, $y_j = \cos(j\Delta\theta - \frac{1}{2}\Delta\theta)$ . It can be found that the influence coefficients $I_{1,i,j}$ and $I_{2,i,j}$ are irrespective of time and can thus be integrated once and for all.

### 2.2. Modified Linear Solution

It's relatively time-consuming to compute the nonlinear solution directly. In order to make the final solution in better agreement with the fully nonlinear solution, a correction is required for the linear solution. Madsen et al. [6] suggested a simple correction by multiplying the velocities from the linear solution $w_x$ and $w_y$ with the factor

$$k_a = \frac{1}{1-a} \tag{18}$$

where the induction factor $a$ is found based on a relationship between the induction $a$ and the average thrust coefficient $C_T$. A polynomial relationship [3] between $C_T$ and $a$ used in the practical implementation for HAWT's in HAWC2 was adopted, as given in Eq. 19.

$$a = k_3C_T^3 + k_2C_T^2 + k_1C_T + k_0 \tag{19}$$

in which $k_3 = 0.0892074$, $k_2 = 0.0544955$, $k_1 = 0.251163$ and $k_0 = -0.0017077$. This polynomial includes the $C_T = 4a(1-a)$ for $a < 0.5$ as well as the Glauert correction for $a > 0.5$.

However, implementation using the above modified linear solution shows some deviations in the power coefficients at high tip speed ratios, as the results of the code AC3 shown in Fig. 8. This implies that at large tip speed ratio, such a modification can cause large deviations in the power coefficient, thus a new modification that corrects the $k_a$ at high induction factor, which corresponds to large tip speed ratio, is proposed, as follows.

$$k_a = \begin{cases} \frac{1}{1-a}, & (a \le 0.15) \\ \frac{1}{1-a}(0.65 + 0.35\exp\left(-4.5(a-0.15)\right)), & (a > 0.15) \end{cases} \tag{20}$$

in which the empirical parameters are determined by comparing with the experimental data, as illustrated in Fig. 8.

## 3. Aerodynamic loads on a 2D VAWT

The aerodynamic loads acting on a 2D VAWT according to the AC flow method can be calculated as follows. The local inflow velocity seen at a blade section is computed by adding the free wind speed and the induced velocity and subtracting the velocity due to the motion. Consequently, the relative velocity and angle of attack experienced by the section are found and the corresponding aerodynamic coefficients are determined using a look-up table in terms of the angle of attack. In this way the normal and tangential loads acting on the cylinder can be determined. In this study two approaches are used to determine the normal and tangential loads acting on the rotor, namely:

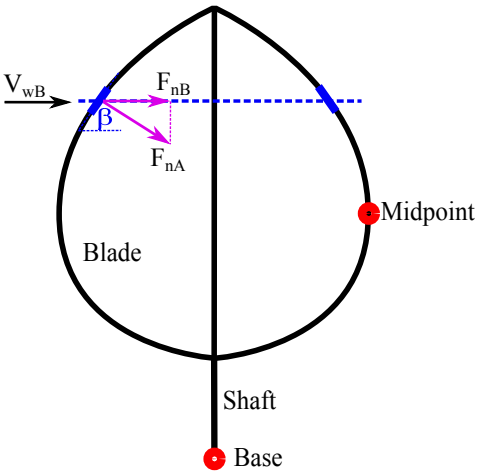


Fig. 3. An illustration of the local element force acting on the blade of a VAWT.

- Approach I:

$$Q_t = \frac{BF_{tB}}{2\pi R\rho V_{wB}^2} \tag{21}$$

$$Q_n = \frac{BF_{nB}}{2\pi R\rho V_{wB}^2} \tag{22}$$

- Approach II:

$$Q_t = \frac{BF_{tA}}{2\pi R\rho V_{wB}^2 \sin(\beta)} \tag{23}$$

$$Q_n = \frac{BF_{nA}}{2\pi R\rho V_{wB}^2 \sin(\beta)} \tag{24}$$

where $B$ is the number of blades, $R$ the radius of the disk considered, $\beta$ the blade angle with the vertical direction, and $V_{wB}$ the local free wind speed.

Approach I is based on the assumption that the local element considered is parallel to the rotating shaft, while approach II takes into account the inclination of the local element, which can represent more physical phenomena if the blade is curved or helical. The average thrust coefficient used in Eq. 19 can then be computed using $Q_n$ and $Q_t$.

## 4. Aerodynamic modeling of a floating VAWT using the AC method

The flow chart of the aerodynamic modeling of a floating VAWT using the AC method is shown in Fig. 4. A swept surface is created when a VAWT rotates. A set of cylinders along the shaft is obtained by dividing the swept surface vertically, and for each cylinder a number of grids coinciding with the swept surface can then be obtained by dividing the cylinder circumferentially. In this sense the flow expansion in the vertical direction is not considered. A typical number of 20-30 cylinders along the shaft and 36 azimuth angles for each cylinder is recommended by [6]. At each time step, the induced velocity coefficients at these grids can be computed based on the AC method described above. Thus the induced velocity at the actual calculation point for each blade can then be determined using an linear interpolation from two nearest grids to the considered calculation point. The effect of dynamic stall is also included using the Beddoes-Leishman dynamic stall model. The effects of wind shear and turbulence if present can be included by the local free wind speed.

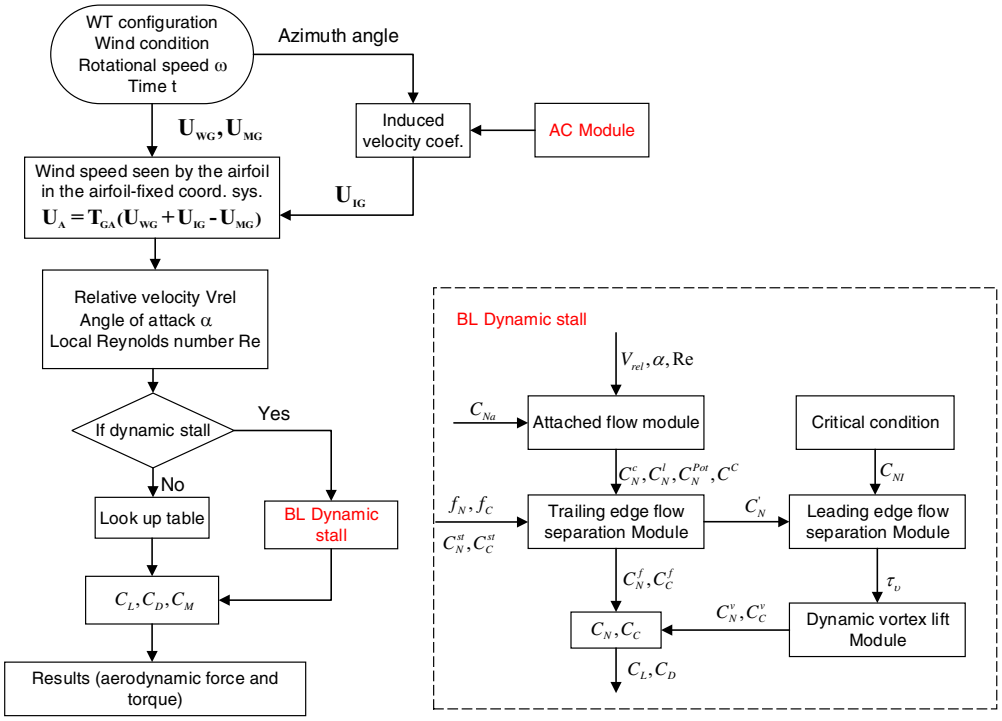


Fig. 4. Flow chart for aerodynamic modeling of a floating VAWT using the AC method. Here $\mathbf{U_{WG}}$, $\mathbf{U_{IG}}$ and $\mathbf{U_{MG}}$ are global wind speed, induced velocity and velocity due to motion, respectively. $\mathbf{T_{GA}}$ is the transform matrix from global coordinate system to the air-foil fixed coordinate system. Other parameters involved can refer to [1].

## 5. Verifications

An aerodynamic code is developed to model offshore VAWTs using the AC method. In this section, a series of comparisons against numerical models and experimental results are carried out to verify the accuracy of the developed code. Based on the combination of the approaches for the normal and tangential loads, the option for including or neglecting the $Q_t$ term in Eqs. 14 and 15 when calculating the induced velocity, and different modified linear solutions, the AC codes developed can be categorized into AC1, AC2, AC3 and AC4, as given in Table 1.

Table 1. Different AC codes

| | Approach for $Q_n$ and $Q_t$ | $Q_t$ term in Eqs. 14 and 15 | Modified linear solution |
|---|---|---|---|
| AC1 | I | Neglected | Eq. 18 |
| AC2 | I | Included | Eq. 18 |
| AC3 | II | Included | Eq. 18 |
| AC4 | II | Included | Eq. 20 |

### *5.1. Verification of the codes AC1 and AC2*

The codes AC1 and AC2 compute the aerodynamic loads based on the approach I for the normal and tangential loads. In this study the codes are verified by comparing with the numerical results by Larsen and Madsen [3]. A 5MW

Darrieus rotor with the radius of 64.96 m and height of 130 m was adopted. Various simulations were conducted using the linear solution and modified linear solution. The steady wind with a wind speed of 9 $m/s$ was used and the tip speed ratio $\lambda$ was set to be 3. The airfoil NACA0015 with the same aerodynamic coefficients were employed in all simulations.

Fig. 5 presents the normal loading $Q_n$ and tangential loading $Q_t$ at the midpoint of the blade (as shown in Fig. 3 ) along the cylinder periphery when the effect of induced velocities is not considered. Larsen and Madsen [3] carried out the simulations using the AC code and the HAWC2 code, respectively. It shows that these codes agree very well on the normal loading. Regarding the tangential loading, the present AC code agrees well with the result of the HAWC2 code.

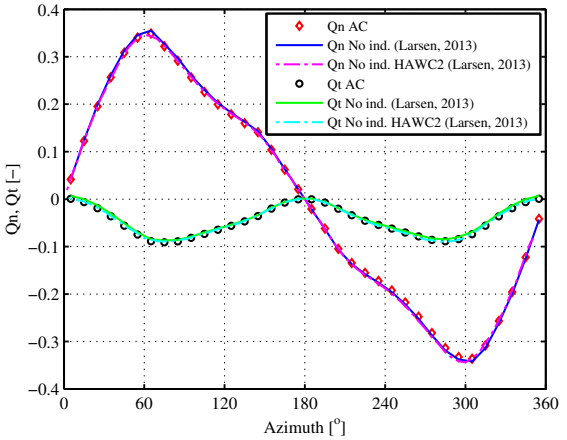


Fig. 5. Normal loading $Q_n$ and tangential loading $Q_t$ at the midpoint of the blade (as shown in Fig. 3 ) along the cylinder periphery for $\lambda = 3$. The effect of induced velocities is not considered.

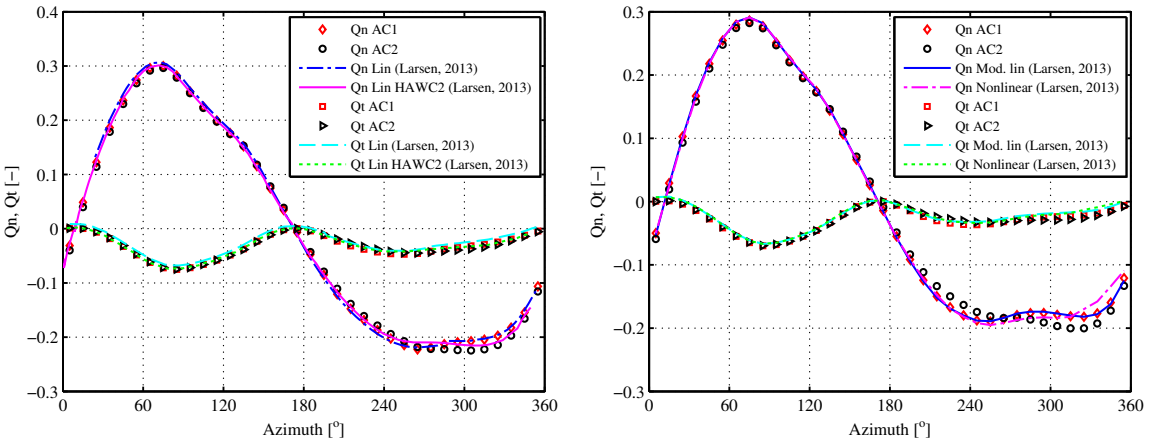


(a) With linear solution (b) With modified linear solution

Fig. 6. Normal loading $Q_n$ and tangential loading $Q_t$ at the midpoint of the blade ( as shown in Fig. 3 ) along the cylinder periphery predicted using the linear solution and modified linear solution for $\lambda = 3$. Differences between the codes AC1 and AC2 can refer to Table 1.

Linear solution is then used to predict the normal and tangential loading on the rotor. Fig. 6 (a) demonstrates the normal loading $Q_n$ and tangential loading $Q_t$ at the midpoint of the blade along the cylinder periphery. Here the AC1 and AC2 code are applied and the difference between these two AC codes lies in that for the code AC1 the $Q_t$ term in

Eqs. 14 and 15 is neglected when calculating the induced velocity. It should also be noted that both the linear solution in the AC by [3] and the implementation of AC method in HAWC2 ignores the $Q_t$ term in Eqs. 14 and 15.

In the windward part, both the normal and tangential loads resulting from AC1, AC2 and the HAWC2 implementation are very close. However, in the leeward part, especially in the vicinity of azimuth angle of 270 $^o$, those codes present relatively large differences with respect to the normal and tangential loads. The codes AC1 and AC2 predict a little larger tangential load than the HAWC2 implementation. Regarding the codes AC1 and AC2, the AC2 gives a little smaller normal and tangential loads in the first and third quadrants and a little larger normal and tangential loads in the second and fourth quadrants. This is due to the effect of including tangential loads when calculating the induced velocity.

In order to predict the aerodynamic loads accurate at a small computational cost, a modified linear solution proposed by Madsen et al. [6] is used. Fig. 6(b) compares the normal loading $Q_n$ and tangential loading $Q_t$ at the midpoint of the blade along the cylinder periphery using the codes AC1 and AC2. The nonlinear solution considered by Larsen and Madsen [3] neglects the effect of tangential loads when calculating the induced velocity.

The normal load computed by AC1 agrees quite well with that of the modified linear solution by Larsen and Madsen [3]. But the AC1 predicts a little larger tangential loads than the modified linear solution by Larsen and Madsen [3], especially in the downwind part. With respect to the code AC2, deviations between the AC2 and modified linear solution of Larsen and Madsen [3] are both observed in the normal and tangential loads, particularly in the downwind part of the rotor, since the terms of tangential loads are included in AC2 when calculating the induced velocity.

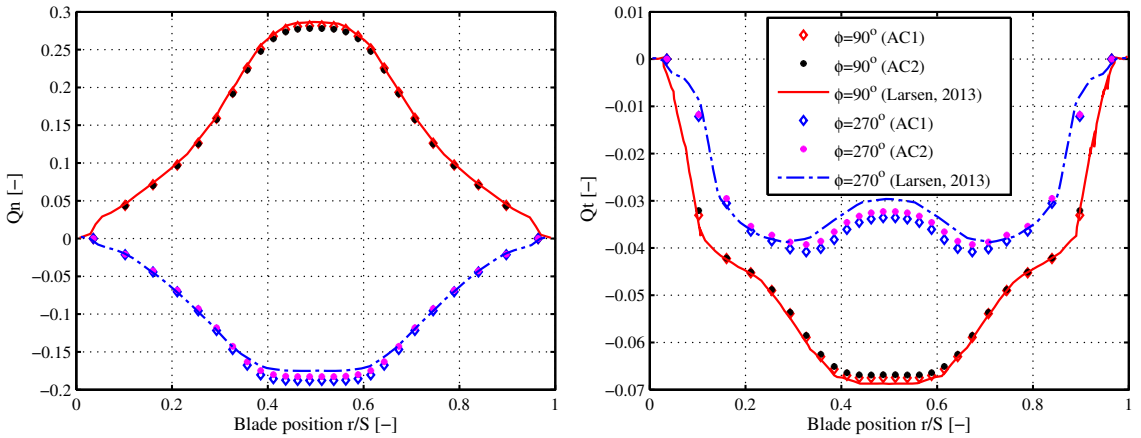


Fig. 7. Distribution of the normal load $Q_n$ and tangential load $Q_t$ as a function of position on the blade at azimuth angle of 90$^o$ and 270$^o$. Differences between the codes AC1 and AC2 can refer to Table 1.

The above verifications are with respect to the midpoint of the blade. It's also necessary to investigate and verify the distribution of normal and tangential loads along the blade at different azimuth angles, as shown in Fig. 7. At the azimuth angle of 90$^o$, both the normal and tangential loads predicted by the codes AC1, AC2 and the implementation in HAWC2 by Larsen and Madsen [3] are very close. While at the azimuth angle of 270$^o$, these codes shows small differences in the middle part of the blade , with the position $r/S$ approximately ranging from 0.3 to 0.7. Moreover, the AC2 gives a little smaller normal and tangential loads than the AC1.

As a whole, the present codes AC1 and AC2 agree well with the results in Larsen and Madsen [3] and can be regarded to be accurate enough to model floating VAWTs.

### 5.2. *Verification of the codes AC3 and AC4*

The codes AC3 and AC4 calculate the normal and tangential loads using approach II with different method to correct the linear solutions. In this study the codes AC3 and AC4 are verified by comparison with experiment data. Two rotors are considered here, i.e. the 3-bladed Sandia 5 m Darrieus rotor and 2-bladed Sandia 17 m Darrieus rotor. The power coefficient at different tip speed ratio for these two rotors are demonstrated in Fig. 8. It's obvious that at

low tip speed ratio, the codes AC3 and AC4 match well with each other and also agree well with the experimental data; However, at high tip speed ratio, the code AC4 can predict the power accurately while the code AC3 underestimates it. The modified linear solution proposed in this paper can better predict the aerodynamic power.

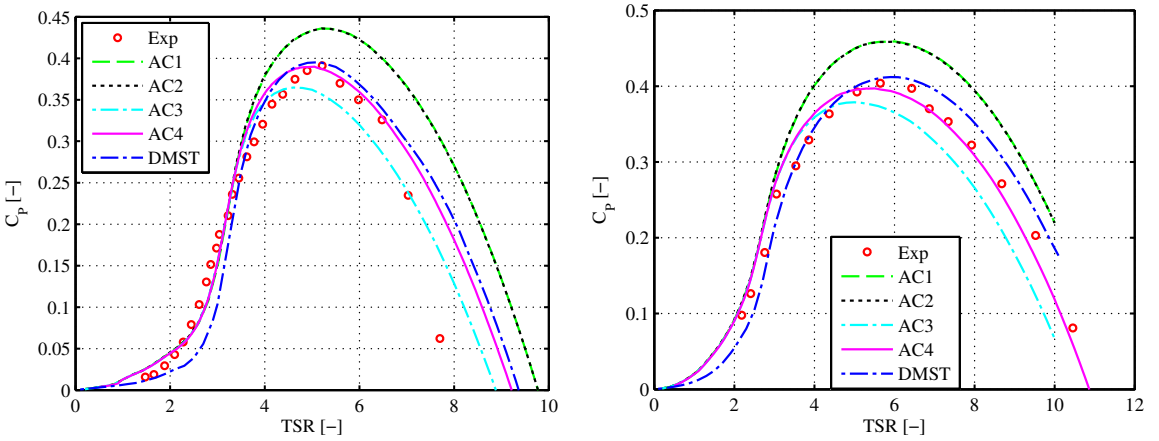


(a) The 3-bladed Sandia 5 m Darrieus rotor

(b) The 2-bladed Sandia 17 m Darrieus rotor

Fig. 8. Comparison of power coefficient curve between simulation model and experimental data. (a): the 3-bladed Sandia 5 m Darrieus rotor at rotational speed of 150 rpm, (b): the 2-bladed Sandia 17 m Darrieus rotor at rotational speed of 50.6 rpm. Differences between the codes AC1, AC2, AC3 and AC4 can refer to Table 1.

## 6. Comparison of the AC and DMST methods

Fig. 8 also show comparisons between the developed AC methods and the DMST method. It can be found that at a low tip speed ratio, which corresponds to small axial induction factor, the codes AC1, AC2, AC3 and AC4 are very close and can all predict the aerodynamic power accurately; and the DMST method seems to underpredict the aerodynamic power to some extent. At a high tip speed ratio, the AC1, AC2 and DMST codes overestimate the aerodynamic power, whereas the code AC3 underestimates the aerodynamic power.

In order to illustrate the difference between each code, the coefficients of thrust, lateral force and aerodynamic torque of the Sandia 17 m Darrieus rotor are also studied, as shown in Fig. 9. Two representative tip speed ratio are considered here. At a low tip speed ratio, for instance $\lambda = 2.5$, all these codes predict very close aerodynamic torque, but the DMST method differs in thrust and side force from the AC method since it ignores the induction in the cross-flow direction. Moreover, the aforementioned two approaches used to calculate the normal and tangential loads have very small difference at the low tip speed ratio. At a high tip speed ratio, for example $\lambda = 7$, the codes AC1 and AC2 overpredict the thrust and aerodynamic torque significantly, while the code AC3 gives a little smaller thrust and aerodynamic torque than the code AC4. When comparing the results of the codes AC4 and DMST, the DMST method overpredicts a little the aerodynamic torque but underestimates the thrust.

## 7. Conclusions

This paper deals with the aerodynamic modeling of floating VAWTs using the Actuator Cylinder (AC) method. An aerodynamic code has been developed to calculate the aerodynamic loads acting on the blades of VAWTs considering the shear and turbulent wind as well as the effect of dynamic stall using the Beddoes-Leishman dynamic stall model. Currently, the flow expansion of the induced velocity in the vertical direction is not considered.

The aerodynamic modeling of VAWTs are studied in depth in this paper. Linear solutions of the induced velocities along the cylinder are firstly derived to account for the effect of tangential load. Two different approaches are used to

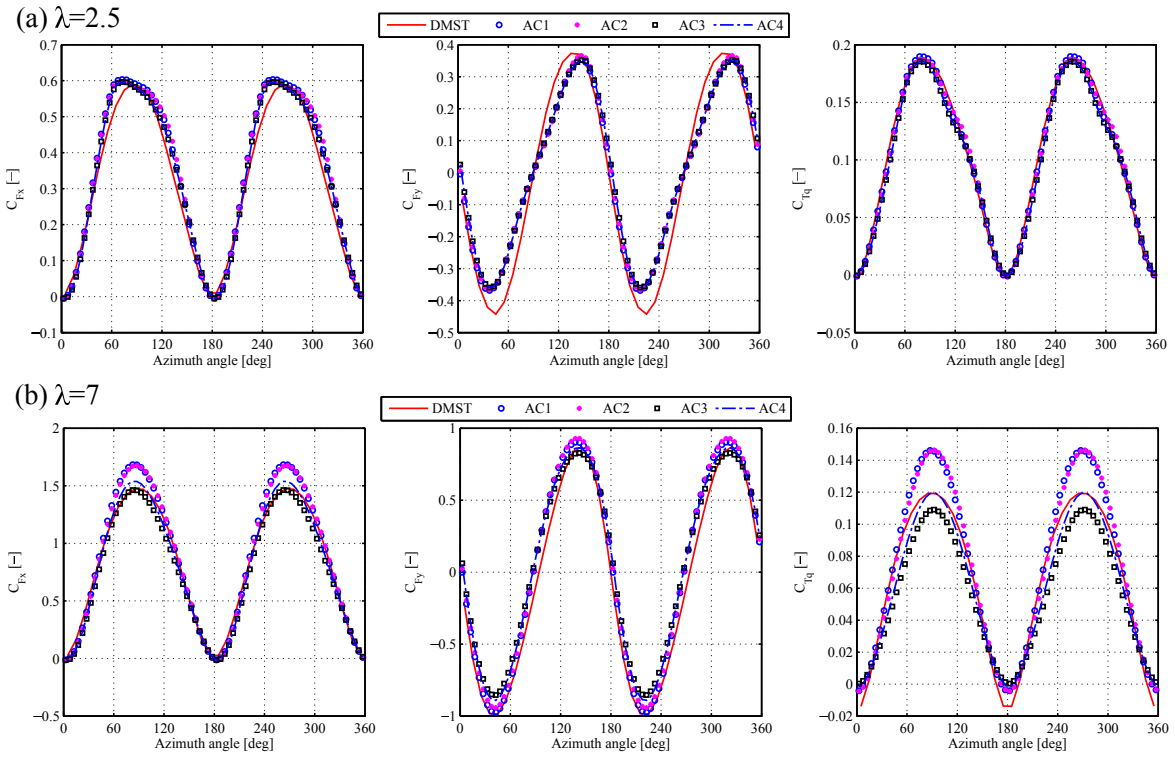


Fig. 9. Coefficients of thrust, side force and torque for the Sandia 17 m Darrieus rotor as a function of the azimuth angle. The effect of dynamic stall is not included. Differences between the codes AC1, AC2, AC3 and AC4 can refer to Table 1.

calculate the normal and tangential loads along the cylinder. Moreover, two different modifications are employed to correct the linear solution of the induced velocities.

The effect of tangential load on the aerodynamic loads when calculating the induced velocities is found to be relatively very small. Calculating the normal and tangential loads using approach II which considers more physical phenomena predicts better aerodynamic loads than approach I. Moreover, the modified linear solution proposed in this study gives very good aerodynamic power prediction compared with experimental data.

In addition, comparative studies of the developed AC codes and the double multi-streamtube (DMST) method are carried out and show that the developed AC method, which includes the tangential load term when calculating the induced velocities, computes the normal and tangential loads using approach II and employs the new modified linear solution, can predict more accurate aerodynamic power and aerodynamic loads than the DMST method.

The developed AC method is found to be accurate for modeling offshore VAWTs. This AC code can be integrated with the computer codes SIMO-RIFLEX to form a fully coupled simulation tool, i.e. SIMO-RIFLEX-AC [1], which is capable of performing the aero-hydro-servo-elastic time-domain analysis for offshore bottom-fixed or floating VAWTs.

## Acknowledgments

The authors would like to acknowledge the financial support from the EU FP7 project MARE WINT (project NO. 309395) and the Research Council of Norway through the Centre for Ships and Ocean Structures (CeSOS) and Centre for Autonomous Marine Operations and Systems (AMOS) at the Department of Marine Technology, Norwegian University of Science and Technology (NTNU), Trondheim, Norway. The first author would like to thank

the Department of Wind Energy for kindly hosting me and valuable discussions with senior scientist Torben J. Larsen at the Technical University of Denmark, Roskilde, Denmark.

## References

[1] Cheng, Z., Madsen, H. A., Gao, Z., Moan, T., 2016. A fully coupled method for numerical modeling and dynamic analysis of floating vertical axis wind turbines. Prepared for possible journal publication.
[2] Ferreira, C. S., Madsen, H. A., Barone, M., Roscher, B., Deglaire, P., Arduin, I., 2014. Comparison of aerodynamic models for vertical axis wind turbines. Journal of Physics: Conference Series 524 (1), 012125.
[3] Larsen, T. J., Madsen, H. A., 2013. On the way to reliable aeroelastic load simulation on VAWT's. In: Proceedings of EWEA.
[4] Madsen, H. A., 1982. The Actuator Cylinder: A flow model for vertical axis wind turbines. Institute of Industrial Constructions and Energy Technology, Aalborg University Centre.
[5] Madsen, H. A., 1983. On the ideal and real energy conversion in a straight bladed vertical axis wind turbine. Institute of Industrial Constructions and Energy Technology, Aalborg University Centre.
[6] Madsen, H. A., Larsen, T. J., Paulsen, U. S., Vita, L., 2013. Implementation of the actuator cylinder flow model in the HAWC2 code for aeroelastic simulations on vertical axis wind turbines. In: 51st AIAA Aerospace Sciences Meeting including the New Horizons Forum and Aerospace Exposition.
[7] Murray, J., Barone, M., 2011. The development of cactus, a wind and marine turbine performance simulation code. In: 49th AIAA Aerospace Sciences Meeting. Paper AIAA 2011-47.
[8] Paquette, J., Barone, M., 2012. Innovative offshore vertical-axis wind turbine rotor project. EWEA 2012 Annual Event.
[9] Paraschivoiu, I., 2002. Wind turbine design: with emphasis on Darrieus concept. Polytechnic International Press., Montreal, Canada.
[10] Paulsen, U. S., Madsen, H. A., Hattel, J. H., Baran, I., Nielsen, P. H., 2013. Design optimization of a 5 mw floating offshore vertical-axis wind turbine. Energy Procedia 35, 22–32.
[11] Roscher, B., 2014. Current aerodynamic models for VAWT and numerical comparison between HAWC2 and U2DiVA. Special project - EWEM rotor design.
[12] Strickland, J. H., 1975. The darrieus turbine: A performance prediction model using multiple streamtubes. Technical Report SAND75-0430 , Sandia National Laboratories, Albuquerque, N.M. USA.
[13] Templin, R. J., 1974. Aerodynamic performance theory for the nrc vertical-axis wind turbine. Technical Report LTR-LA-160, National Aeronautical Establishment, Ottawa, Ontario, Canada.

## Appendix A. Linear solution of the AC flow problem

In Eq. 5, let $\xi = -r\sin\theta, \eta = r\cos\theta$, we have

$$\begin{aligned} p_f =& \lim_{\epsilon\to 0}\frac{1}{2\pi}\int_{1-\epsilon}^{1+\epsilon}\int_0^{2\pi}\frac{(-f_n\sin\theta - f_t\cos\theta)(x + r\sin\theta) + (f_n\cos\theta - f_t\sin\theta)(y - r\cos\theta)}{(x + r\sin\theta)^2 + (y - r\cos\theta)^2} r dr d\theta \\ =& \frac{1}{2\pi}\int_0^{2\pi} Q_n(\theta)\frac{-(x + \sin\theta)\sin\theta + (y - \cos\theta)\cos\theta}{(x + \sin\theta)^2 + (y - \cos\theta)^2} d\theta \\ &+ \frac{1}{2\pi}\int_0^{2\pi} Q_t(\theta)\frac{-(x + \sin\theta)\cos\theta - (y - \cos\theta)\sin\theta}{(x + \sin\theta)^2 + (y - \cos\theta)^2} d\theta \end{aligned} \tag{A.1}$$

For the integral part in Eq. 3, since the volume forces are non-zero only along the cylinder, the integral result depends on the position of the calculation point.

- When the calculation point is located inside the cylinder, as the point $P_1(x, y)$ shown in Fig. 2, the integral part can be written as

$$\int_{-\infty}^{x} f_x dx' = \int_{-\infty}^{0} f_x dx'$$

note that $x' = -\sqrt{r^2 - y^2}$ , $dx' = -\frac{r}{\sqrt{r^2-y^2}}dr$, and $f_x = -f_n\sin\theta - f_t\cos\theta = -f_n\frac{\sqrt{r^2-y^2}}{r} - f_t\frac{y}{r}$, this yields

$$\begin{aligned}\int_{-\infty}^{x} f_x dx' &= \lim_{\epsilon\to 0}\int_{1+\epsilon}^{1-\epsilon}\left(-f_n\frac{\sqrt{r^2-y^2}}{r}-f_t\frac{y}{r}\right)\left(-\frac{r}{\sqrt{r^2-y^2}}\right)dr\\ &= -\lim_{\epsilon\to 0}\int_{1-\epsilon}^{1+\epsilon}\left(f_n+f_t\frac{y}{\sqrt{r^2-y^2}}\right)dr\\ &= -Q_n(\arccos y)-Q_t(\arccos y)\frac{y}{\sqrt{1-y^2}}\end{aligned} \tag{A.2}$$

- When the calculation point is located at the leeward part of the cylinder, as the point $P_2(x, y)$ shown in Fig. 2, the integral part can be written as

$$\int_{-\infty}^{x} f_x dx' = \int_{-\infty}^{0} f_x dx' + \int_{0}^{x} f_x dx'$$

The first term in the right hand side of the equation has been computed above. For the second term in the right hand side, since $x' > 0$ then $x' = \sqrt{r^2-y^2}$, we have $dx' = \frac{r}{\sqrt{r^2-y^2}}dr$ and $f_x = -f_n\sin\theta - f_t\cos\theta = f_n\frac{\sqrt{r^2-y^2}}{r} - f_t\frac{y}{r}$

$$\begin{aligned}\int_{0}^{x} f_x dx' &= \lim_{\epsilon\to 0}\int_{1-\epsilon}^{1+\epsilon}\left(f_n\frac{\sqrt{r^2-y^2}}{r}-f_t\frac{y}{r}\right)\left(\frac{r}{\sqrt{r^2-y^2}}\right)dr\\ &= \lim_{\epsilon\to 0}\int_{1-\epsilon}^{1+\epsilon}\left(f_n-f_t\frac{y}{\sqrt{r^2-y^2}}\right)dr\\ &= Q_n(-\arccos y)-Q_t(-\arccos y)\frac{y}{\sqrt{1-y^2}}\end{aligned} \tag{A.3}$$

Regarding the integration in Eq. 4, it should be noted that [4]

$$\int_{-\infty}^{x}\frac{\partial p_f}{\partial y}dx' = \frac{1}{2\pi}\iint\frac{-f_y(x-\xi)+f_x(y-\eta)}{(x-\xi)^2+(y-\eta)^2}d\xi d\eta + \int_{-\infty}^{x} f_y dx' \tag{A.4}$$

Therefore,

$$\begin{aligned}w_y(f) &= -\int_{-\infty}^{x}\frac{\partial p_f}{\partial y}dx' + \int_{-\infty}^{x} f_y dx'\\ &= -\frac{1}{2\pi}\iint\frac{-f_y(x-\xi)+f_x(y-\eta)}{(x-\xi)^2+(y-\eta)^2}d\xi d\eta\\ &= -\frac{1}{2\pi}\int_0^{2\pi} Q_n(\theta)\frac{-(x+\sin\theta)\cos\theta-(y-\cos\theta)\sin\theta}{(x+\sin\theta)^2+(y-\cos\theta)^2}d\theta\\ &\quad+\frac{1}{2\pi}\int_0^{2\pi} Q_t(\theta)\frac{-(x+\sin\theta)\sin\theta+(y-\cos\theta)\cos\theta}{(x+\sin\theta)^2+(y-\cos\theta)^2}d\theta\end{aligned} \tag{A.5}$$

In this way, the integration in Eqs. 3 and 4 can be conducted and the linear solution of the velocities can be obtained.